Momentum-resolved above-threshold ionization of deuterated water

Chuan Cheng , Ruaridh Forbes, Andrew J. Howard, Amichael Spanner, Amichael Spanner, Philip H. Bucksbaum, And Thomas Weinacht Department of Physics, Stony Brook University, Stony Brook, New York 11794, USA

Stanford PULSE Institute, SLAC National Accelerator Laboratory, 2575 Sand Hill Road, Menlo Park, California 94025, USA

Department of Physics, Stanford University, Stanford, California 94305, USA

Department of Applied Physics, Stanford University, Stanford, California 94305, USA

National Research Council of Canada, 100 Sussex Drive, Ottawa, Canada K1A 0R6

Department of Physics, University of Ottawa, Ottawa, Canada K1N 6N5



(Received 7 April 2020; accepted 19 October 2020; published 16 November 2020)

We present momentum-resolved coincidence measurements of strong-field single and double ionization of deuterated water (D_2O) using intense few-cycle laser pulses. We measure the vector momentum of electrons and ions resulting from the laser-molecule interaction. This enables us to measure the photoelectron spectrum for electrons in coincidence with fragment ions having different momenta, which can be related to different final states of the cation and dication. The photoelectron spectra for different fragment ion momenta show striking differences, which can be interpreted in terms of the removal of electrons from different molecular orbitals, including the highest occupied molecular orbital (HOMO), as well as more deeply bound ones (e.g., HOMO-2). We discuss our measurements in light of calculations which model the strong-field light matter interaction.

DOI: 10.1103/PhysRevA.102.052813

I. INTRODUCTION

Strong-field ionization is a cornerstone of attosecond science [1] and a key tool in probing molecular structure and dynamics [2–6]. It produces attosecond bursts of current, which can lead to attosecond soft x-ray pulses [7,8] and launch entangled electron-nuclear wave packets in small molecules [3,9,10]. The coupled motion of electrons and nuclei following strong-field ionization has wide ranging implications for molecular science and provides an excellent testbed for understanding nonadiabatic dynamics in molecules [11,12].

The tools for investigating strong-field processes have evolved from simple studies of ionization vs intensity or pulse duration [13,14], to coincidence measurements of charged particle momenta [15]. Measurements of ionization vs photon energy [16], intensity [17–20], polarization [21], and channel (final-state-resolved) [22–25] have shed light on many aspects of the ionization dynamics, such as the role of electron correlation in nonsequential double ionization [15,26–28], the importance of Stark-shifted resonance enhancement [29], and tunnel ionization from inner orbitals [22,30–34].

Here we consider strong-field ionization from multiple orbitals of water using vector momentum-resolved coincidence measurements of both electrons and ions. Water was chosen as a nonlinear polyatomic system of universal interest. Working with a deuterated sample (D_2O) allowed us to measure D^+ fragments more readily than H^+ given our switching coincidence apparatus. We find strong correlations between the momentum of fragment ions and the structure of the photoelectron spectrum, which encodes information on the ionized orbital. Electrons in coincidence with some fragment

momenta indicate electron removal from a single molecular orbital, while electrons in coincidence with other fragment momenta indicate removal of electrons from more than one orbital. We find that the differences in the peak positions for the separate channel-resolved ATI (above-threshold ionization) spectra closely match the energy differences of the first three states of the cation (modulo the photon energy), suggesting that there is no difference in the ponderomotive shifts for the different channels. We compare our measurements with calculations that solve the time-dependent Schrödinger equation (TDSE) for the molecule in the strong laser field, yielding angle and state resolved yields [35,36].

II. EXPERIMENTAL SETUP

The experimental setup has been described in detail in previous work [37,38]. Briefly, the output from a commercial amplified Ti:sapphire laser system (KM Labs, 1 mJ, 780 nm, 1 kHz) is spectrally broadened to 200 nm using filamentation in Ar gas, and compressed to ~ 10 fs using chirped mirrors and an acousto-optic pulse shaper [39]. The pulses are focused by a concave spherical silver mirror (f = 5 cm) to a peak intensity of 400 TW/cm² inside a velocity map imaging (VMI) spectrometer. The VMI has a switchable three plate electrostatic lens stack, microchannel plate (MCP), phosphor screen, and camera (Timepix3). The 1 ns resolution of the Timepix3 camera can resolve the three-vector momenta of ions, or two-dimensional (2D) electron momenta projected on the plane of the detector. The intensity is calibrated using the VMI to measure the classical $2U_p$ cutoff for field-ionized electrons from argon [40].

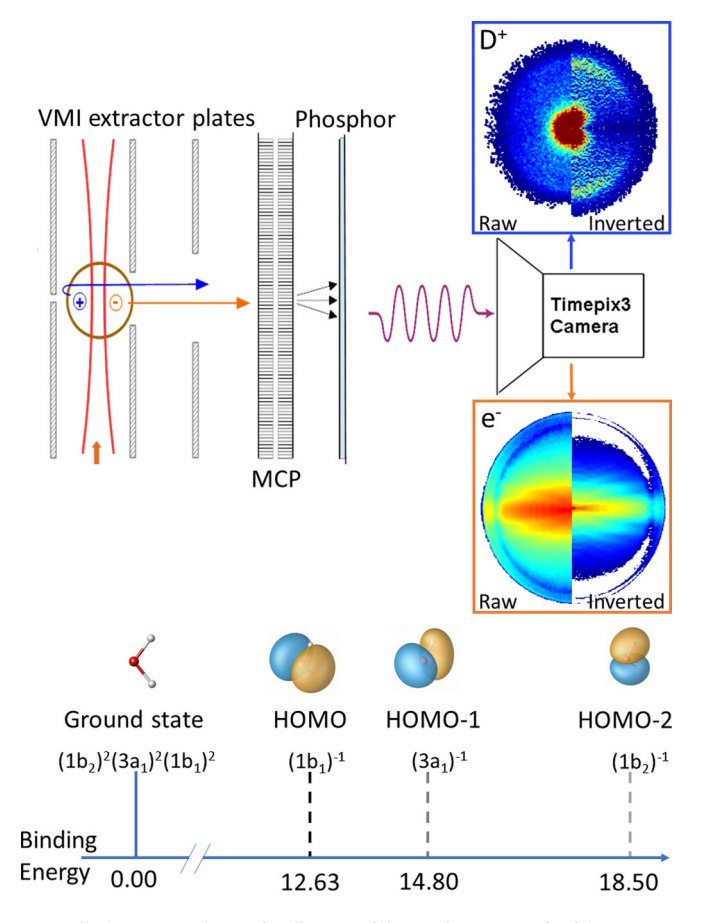


FIG. 1. Top: schematic diagram illustrating our coincidence velocity map imaging (VMI) apparatus which makes use of a Timepix3 Camera. A high voltage pulser is used to switch the accelerating field voltage in order to detect both electrons and ions in coincidence. Shown are the sample images of D⁺ ions (upper) and photoelectrons (lower) in two different views: raw image (left) and Abel inverted image (right). A detailed description of the apparatus is outlined in Refs. [37,38,42]. Bottom: orbital shapes, configurations, and binding energies for the removal of the three most weakly bound electrons [2,43].

A skimmed molecular beam of the target D_2O molecules intersects the laser in the interaction region of the VMI [37]. Switching the voltages on the VMI plates after the detection of the electrons permits VMI measurements of the ions from the same ionization event [38]. The top half of Fig. 1 illustrates this coincidence VMI apparatus.

III. RESULTS AND DISCUSSION

Here we focus on photoelectrons that are measured in coincidence with specific ionic fragment vector momenta. These ionic momenta reveal the ionization channel, which is related to the final mono- or dication state following ionization [38]. The corresponding photoelectron spectra contain information on the orbital(s) from which the electrons are removed [41]. The *combined* information identifies which orbital vacancies lead to specific mono- and dicationic channels. We identify and compare photoelectrons from four different ionization channels: single nondissociative ionization to

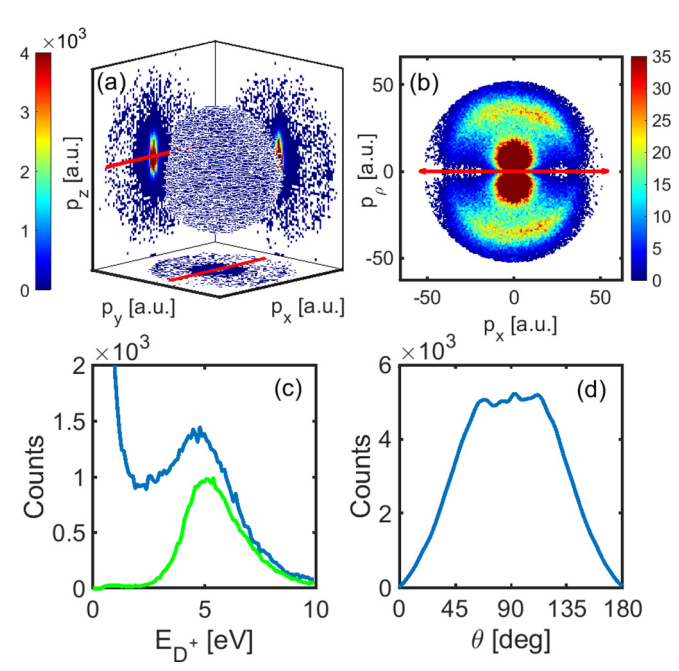


FIG. 2. D^+ momentum and energy spectra. Panel (a) shows the full 3D view of the D^+ ion with three different slices $(p_x p_z, p_y p_z, and p_x p_y)$ on the sides. Panel (b) shows a two-dimensional projection of the momentum distribution in the p_x - p_ρ plane, where the x axis is defined by the laser polarization axis (red) and $p_\rho = \sqrt{p_y^2 + p_z^2}$. These two top panels use the same scale. Panel (c) shows the yield as a function of kinetic energy of the D^+ ion [blue (dark gray)], together with the scaled yield of the D^+ ion in coincidence with OD^+ ions [green (light gray)], while panel (d) shows the D^+ ion yield as a function of angle θ with respect to polarization axis for data in the 5 eV peak in panel (c).

form D_2O^+ , single dissociative ionization to form low-energy D^+ , double ionization to low-lying states of the dication which result in two-body dissociation, producing D^+/OD^+ , and finally double ionization with three-body decay to produce $D^+/O/D^+$.

The D_2O^+ parent ion is formed by removing one electron from the HOMO or HOMO-1, leading to the only configurations that correspond to nondissociative states of the monocation [43–45]. Removal of a HOMO-2 electron leads to dissociation. All dication states are unstable [46] and lead to either two-body dissociation (D⁺/OD⁺), mostly from the first three states of the dication [47], or three-body dissociation (D⁺/O/D⁺) [47,48].

Figure 2 shows the distribution of D⁺ fragment momenta. The full 3D momentum distribution shown in Fig. 2(a) is measured directly with the Timepix3 camera and constructed without employing an inverse Abel transformation by using the position of hits on the camera for the transverse momentum and the timing for the longitudinal momentum. The momentum distribution has a low-momentum concentration and an outer shell, readily seen in the cylindrical projection in Fig. 2(b).

Further projection on D^+ kinetic energy and angle with respect to the laser polarization have been plotted in Figs. 2(c) and 2(d), respectively. The D^+ spectrum in Fig. 2(c) has a low-energy peak, a second peak at around 5 or 6 eV with a

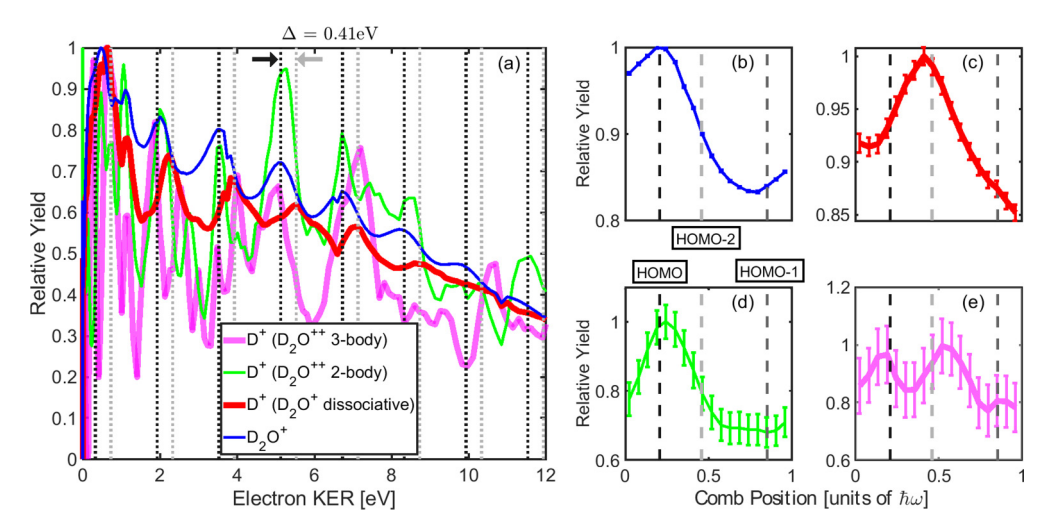


FIG. 3. Panel (a): photoelectron spectra for electrons measured in coincidence with different ions. The four spectra show photoelectrons measured in coincidence with D_2O^+ [thin, blue (dark gray)], low energy (\leq 1 eV) D^+ [thick, red (dark gray)], D^+ arising from two-body breakup of the dication [thin, green (light gray)], and D^+ arising from three-body breakup of the dication [thick, pink (light gray)]. Panels (b) through (e) show the reduced photoelectron spectra as well as error bars described in the text: (b) in coincidence with D_2O^+ ions (nondissociative monocation), (c) in coincidence with low energy D^+ cations (dissociative monocation), (d) in coincidence with D^+ from the dicationic two-body channel, and (e) in coincidence with D^+ from the dicationic three-body channel. Dashed vertical lines illustrate the expected positions of the peaks for the removal of HOMO, HOMO-1, and HOMO-2 electrons (black, intermediate black and grey, respectively).

maximum yield orthogonal to the laser polarization axis, and a broad distribution of ions from 1 to 10 eV. A similar spectrum for the D^+ ion in coincidence to OD^+ (orange) has been plotted indicating that the maximum peak is coming from two-body double ionization. In brief, these energetic features arise from dissociative single ionization (D^+/OD) for D^+ energy ≤ 1 eV, two-body breakup double ionization (D^+/OD^+) for D^+ energies around 5 eV, and three-body breakup double ionization $(D^+/O/D^+)$ for the rest of the D^+ ion [49].

Figure 3(a) shows the photoelectron spectra measured in coincidence with D_2O^+ or D^+ ions integrated over these three different momentum ranges. The photoelectron spectra are generated by Abel inversion of the measured photoelectrons collected for each ionization channel. ATI combs (peaks spaced by the photon energy) are clearly visible in each of the curves. For double-ionization channels this suggests a sequential ionization process, since rescattering of the first electron should wash out the ATI comb structure for nonsequential double ionization.

The ATI spectra in Fig. 3(a) exhibit clear offsets with respect to each other. The difference in the peak locations for electrons in coincidence with the parent ion and D⁺ from two-body dissociation is in excellent agreement with the binding energy of the HOMO and HOMO-2 orbitals, modulo the photon energy (given in Fig. 1). This is strong evidence that the production of D_2O^+ and low-energy D^+ involves the removal of HOMO or HOMO-2 electrons, respectively, and that the removal of these electrons take place with the same ponderomotive energy [43]. Based on this observation, we mark the expected ATI comb positions in (a) to (e) by knowing the position of HOMO and the binding energies of different states. We note that the peaks do not shift with laser intensity, which is consistent with the ponderomotive shift being the same for ionization to different states of the cation [17]. A detailed analysis of this will be explored in future work.

In addition to the offset of the different ATI combs, there are other differences between the ATI spectra that merit discussion. For instance, the ATI spectrum in coincidence with two-body breakup of the dication shows greater depth of modulation, and more structure for each ATI order. To better view these features, we reduce the ATI comb into a single order $S(E|0 \le E < \hbar\omega)$ by summing up the spectrum modulo the photon energy, $\hbar\omega$.

The results of this approach are shown in Figs. 3(b)–3(e). These panels show reduced spectra for photoelectrons from four different channels, and the spectral peaks line up with the expected peak locations for the removal of HOMO, HOMO-1, and HOMO-2 electrons. Errors on each point have been estimated based on bootstrapping resampling analysis. The good agreement shows that the ATI peaks all have energies consistent with ionization to the three lowest states of the cation, even though we are measuring electrons emitted during double ionization. We conclude that these peaks correspond to the removal of the first electron in double ionization, while the second electron does not lead to separate peaks (corresponding to energy differences between states of the cation and dication), but is rather distributed over a broad range of energies [50–53].

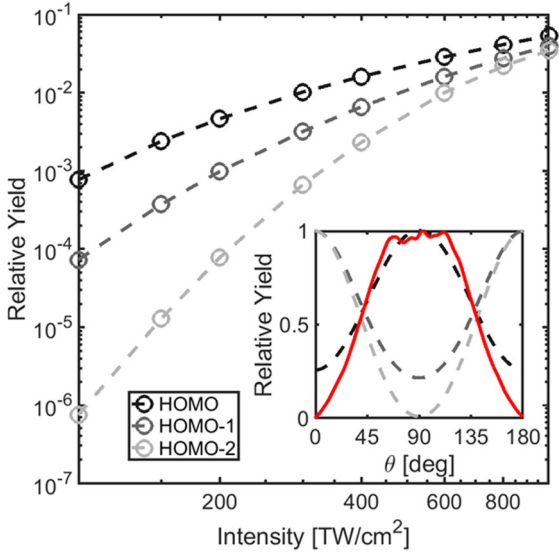
Other features are also evident in the reduced spectra. The spectral positions show that different ionization channels appear to involve electrons from different molecular orbitals: single ionization is dominated by removal of a HOMO electron, as is the double-ionization channel that leads to two-body breakup. Dissociative single ionization appears to follow from removal of a HOMO-2 electron. This indicates that increasing final state energy of ions does not correlate monotonically with the binding energy of the first electron removed by the field. Furthermore, ionization to low-lying states of the cation and dication (producing D_2O^+ and the 5 eV D^+ ions, respectively) involves removal of electrons

from HOMO-1, while ionization to dissociative states of the monocation only shows contributions from HOMO-2, without any contributions from HOMO-1. The presence of both HOMO and HOMO-1 contributions to the ionization producing D_2O^+ is consistent with the fact that both the ground and first excited states of the monocation are nondissociative, leading to the production of D_2O^+ , whereas all higher states are dissociative [43–45]. For the case of the highest-energy channel, double ionization resulting in three-body breakup, the first ionization step involves the removal of an electron from HOMO, HOMO-1, and HOMO-2.

We also note that the varying depth of modulation, peak widths, and offset between the left- and right-hand edges of the comb-analyzed spectra all contain further hints about the ionization dynamics. The large depth of modulation for the spectrum in coincidence with the 5 eV D⁺ ions suggests that sequential double ionization with ATI as the first step plays a large role, and that rescattering (i.e., nonsequential double ionization) is not the dominant mechanism for this channel. The narrow peaks associated with both doubleionization channels are unexpected for our short pulses, and will be investigated further in the future. Finally, the fact that the double-ionization channels show similar yields at the left- and right-hand edges of reduced spectra, while the single-ionization channels do not, simply indicates that the increasing orders of ATI spectra fall off more rapidly for single ionization than they do for double ionization.

To further interpret our measurements, we carried out time-dependent resolution in ionic states (TD-RIS) calculations of the ionization dynamics, solving the TDSE for the molecule in a strong laser field [35,36]. The bound multielectron wave functions for the ground state of the neutral and the lowest three ionic states are computed using the GAMESS electronic structure package [54] with the aug-cc-pVTZ basis set at a CAS MCSCF level of theory, evaluated at the equilibrium geometry of the neutral. The TD-RIS calculations used computational grids extending to ± 15 a.u. with a grid spacing of $\Delta = 0.2$ a.u. The time propagation used a step size of $\delta t = 0.002$ a.u. The ionization yields are calculated by monitoring the outgoing flux that is removed by absorbing boundaries at the edges of the grids [35].

Our TD-RIS calculations indicate that the relative probabilities for removal of HOMO, HOMO-1, and HOMO-2 electrons depend on intensity, and can differ by less than an order of magnitude for the intensities in our experiment. The top panel of Fig. 4 shows the intensity-dependent ionization yield for removal of HOMO, HOMO-1, and HOMO-2 electrons in a half-cycle pulse as a function of intensity and angle (inset). The angle-dependent yield for removal of a HOMO electron is compared with the angle-dependent yield of D+ ions produced in coincidence (cf. Fig. 2). We note that there is good agreement between the calculated and measured angle dependent yields for removal of a HOMO electron. The bottom panel of Fig. 4 shows the calculated angle-dependent yields for all three channels (HOMO, HOMO-1, and HOMO-2) for various laser intensities. These show how the yield is maximum orthogonal to the orbital nodes. In addition, the permanent dipole moment of the molecule combines with the half-cycle pulse used in these calculations to produce a flip in



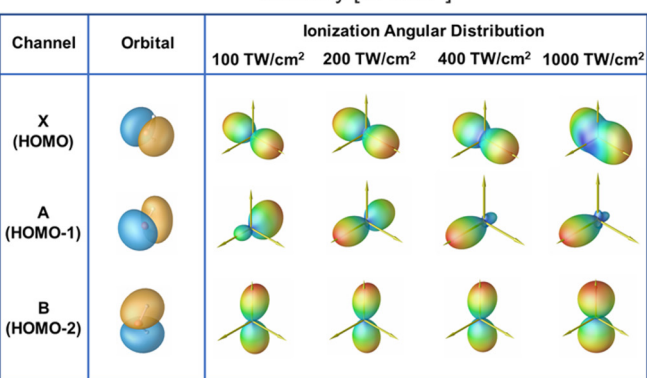


FIG. 4. Top: calculated ionization yields for removal of HOMO, HOMO-1, and HOMO-2 electrons as a function of laser intensity. Top panel inset: black and gray dashed lines show calculated ionization yields for removal of HOMO, HOMO-1, and HOMO-2 electrons as a function of the angle between the laser polarization axis and the molecular plane, while the solid red curve shows the experimentally measured D⁺ yield as a function of the angle between the molecular plane and the laser polarization, as shown in Fig. 2(d). Bottom: angle dependent ionization yields for different channels and laser intensities.

the asymmetry in the ionization yield of HOMO-1 at several intensities.

IV. CONCLUSION

In conclusion, we have studied the strong-field ionization of D_2O with momentum-resolved coincidence measurements of both electrons and ions. From the momentum-resolved ATI (MRATI), we find some fragments are correlated with removal of electrons from more than one orbital. Evidence of sequential double ionization has been shown to play an important role in the strong-field ionization of D_2O . Finally, we compare our measurements with TD-RIS calculations of the ionization dynamics which qualitatively match our measurements.

ACKNOWLEDGMENTS

We would like to thank B. M. Kaufman and Y. Liu for technical support and Z. Streeter, C. W. McCurdy, S. Matsika,

and J. Cryan for useful discussions. R.F., A.J.H., and P.H.B. were supported by the National Science Foundation. A.J.H. was additionally supported under a Stanford Graduate Fel-

lowship as the 2019 Albion Walter Hewlett Fellow. C.C. and T.W. gratefully acknowledge support from the Department of Energy under Award No. DE-FG02-08ER15984.

- [1] P. B. Corkum and F. Krausz, Nat. Phys. 3, 381 (2007).
- [2] J. P. Farrell, S. Petretti, J. Förster, B. K. McFarland, L. S. Spector, Y. V. Vanne, P. Decleva, P. H. Bucksbaum, A. Saenz, and M. Gühr, Phys. Rev. Lett. 107, 083001 (2011).
- [3] H. Niikura, F. Légaré, R. Hasbani, M. Y. Ivanov, D. Villeneuve, and P. Corkum, Nature (London) 421, 826 (2003).
- [4] H. Niikura, F. Légaré, R. Hasbani, A. D. Bandrauk, M. Y. Ivanov, D. M. Villeneuve, and P. B. Corkum, Nature (London) 417, 917 (2002).
- [5] T. Ergler, A. Rudenko, B. Feuerstein, K. Zrost, C. D. Schröter, R. Moshammer, and J. Ullrich, Phys. Rev. Lett. 97, 193001 (2006).
- [6] S. Baker, J. S. Robinson, C. Haworth, H. Teng, R. Smith, C. Chirilă, M. Lein, J. Tisch, and J. P. Marangos, Science 312, 424 (2006).
- [7] M. Hentschel, R. Kienberger, C. Spielmann, G. A. Reider, N. Milosevic, T. Brabec, P. Corkum, U. Heinzmann, M. Drescher, and F. Krausz, Nature (London) 414, 509 (2001).
- [8] P. M. Paul, E. Toma, P. Breger, G. Mullot, F. Augé, P. Balcou, H. Muller, and P. Agostini, Science 292, 1689 (2001).
- [9] D. Geißler, T. Rozgonyi, J. González-Vázquez, L. González, S. Nichols, and T. Weinacht, Phys. Rev. A **82**, 011402(R) (2010).
- [10] Z.-H. Loh and S. R. Leone, J. Chem. Phys. 128, 204302 (2008).
- [11] S. Matsika and P. Krause, Annu. Rev. Phys. Chem. 62, 621 (2011).
- [12] W. Domcke and D. R. Yarkony, Annu. Rev. Phys. Chem. **63**, 325 (2012).
- [13] D. N. Fittinghoff, P. R. Bolton, B. Chang, and K. C. Kulander, Phys. Rev. Lett. 69, 2642 (1992).
- [14] B. Walker, B. Sheehy, L. F. DiMauro, P. Agostini, K. J. Schafer, and K. C. Kulander, Phys. Rev. Lett. 73, 1227 (1994).
- [15] T. Weber, H. Giessen, M. Weckenbrock, G. Urbasch, A. Staudte, L. Spielberger, O. Jagutzki, V. Mergel, M. Vollmer, and R. Dörner, Nature (London) 405, 658 (2000).
- [16] K. J. Schafer, B. Yang, L. F. DiMauro, and K. C. Kulander, Phys. Rev. Lett. 70, 1599 (1993).
- [17] J. Wiese, J.-F. Olivieri, A. Trabattoni, S. Trippel, and J. Küpper, New J. Phys. 21, 083011 (2019).
- [18] T. D. Scarborough, J. Strohaber, D. B. Foote, C. J. McAcy, and C. J. G. J. Uiterwaal, Phys. Chem. Chem. Phys. 13, 13783 (2011).
- [19] T. D. Scarborough and C. G. J. Uiterwaal, Laser Phys. 23, 125302 (2013).
- [20] N. A. Hart, J. Strohaber, G. Kaya, N. Kaya, A. A. Kolomenskii, and H. A. Schuessler, Phys. Rev. A 89, 053414 (2014).
- [21] G. G. Paulus, W. Nicklich, H. Xu, P. Lambropoulos, and H. Walther, Phys. Rev. Lett. 72, 2851 (1994).
- [22] A. E. Boguslavskiy, J. Mikosch, A. Gijsbertsen, M. Spanner, S. Patchkovskii, N. Gador, M. J. J. Vrakking, and A. Stolow, Science 335, 1336 (2012).
- [23] J. Mikosch, A. E. Boguslavskiy, I. Wilkinson, M. Spanner, S. Patchkovskii, and A. Stolow, Phys. Rev. Lett. 110, 023004 (2013).

- [24] A. Zhao, P. Sándor, T. Rozgonyi, and T. Weinacht, J. Phys. B **47**, 204023 (2014).
- [25] P. Sándor, A. Zhao, T. Rozgonyi, and T. Weinacht, J. Phys. B 47, 124021 (2014).
- [26] W. Becker, X. J. Liu, P. J. Ho, and J. H. Eberly, Rev. Mod. Phys. 84, 1011 (2012).
- [27] B. Bergues, M. Kübel, N. G. Johnson, B. Fischer, N. Camus, K. J. Betsch, O. Herrwerth, A. Senftleben, A. M. Sayler, T. Rathje *et al.*, Nat. Commun. 3, 813 (2012).
- [28] L. Zhang, X. Xie, S. Roither, Y. Zhou, P. Lu, D. Kartashov, M. Schöffler, D. Shafir, P. B. Corkum, A. Baltuška *et al.*, Phys. Rev. Lett. 112, 193002 (2014).
- [29] R. R. Freeman, P. H. Bucksbaum, H. Milchberg, S. Darack, D. Schumacher, and M. E. Geusic, Phys. Rev. Lett. 59, 1092 (1987).
- [30] W. Li, X. Zhou, R. Lock, S. Patchkovskii, A. Stolow, H. C. Kapteyn, and M. M. Murnane, Science 322, 1207 (2008).
- [31] B. K. McFarland, J. P. Farrell, P. H. Bucksbaum, and M. Gühr, Science 322, 1232 (2008).
- [32] H. Akagi, T. Otobe, A. Staudte, A. Shiner, F. Turner, R. Dörner, D. M. Villeneuve, and P. B. Corkum, Science 325, 1364 (2009).
- [33] O. Smirnova, Y. Mairesse, S. Patchkovskii, N. Dudovich, D. Villeneuve, P. Corkum, and M. Y. Ivanov, Nature (London) 460, 972 (2009).
- [34] H. Chen, V. Tagliamonti, and G. N. Gibson, Phys. Rev. Lett. 109, 193002 (2012).
- [35] M. Spanner and S. Patchkovskii, Phys. Rev. A 80, 063411 (2009)
- [36] M. Spanner, S. Patchkovskii, C. Zhou, S. Matsika, M. Kotur, and T. C. Weinacht, Phys. Rev. A **86**, 053406 (2012).
- [37] A. Zhao, M. van Beuzekom, B. Bouwens, D. Byelov, I. Chakaberia, C. Cheng, E. Maddox, A. Nomerotski, P. Svihra, J. Visser *et al.*, Rev. Sci. Instrum. **88**, 113104 (2017).
- [38] C. Cheng, P. Vindel-Zandbergen, S. Matsika, and T. Weinacht, Phys. Rev. A 100, 053405 (2019).
- [39] M. A. Dugan, J. X. Tull, and W. S. Warren, J. Opt. Soc. Am. B 14, 2348 (1997).
- [40] P. B. Corkum, Phys. Rev. Lett. 71, 1994 (1993).
- [41] F. Schell, A. E. Boguslavskiy, C. P. Schulz, S. Patchkovskii, M. J. Vrakking, A. Stolow, and J. Mikosch, Phys. Chem. Chem. Phys. 20, 14708 (2018).
- [42] A. Zhao, P. Sándor, and T. Weinacht, J. Chem. Phys. 147, 013922 (2017).
- [43] K. Norwood, A. Ali, and C. Ng, J. Chem. Phys. 95, 8029 (1991).
- [44] X.-M. Qian, Y. Song, K.-C. Lau, C. Ng, J. Liu, W. Chen, and G. He, Chem. Phys. Lett. 353, 19 (2002).
- [45] S. Truong, A. Yencha, A. Juarez, S. Cavanagh, P. Bolognesi, and G. King, Chem. Phys. 355, 183 (2009).
- [46] S. Truong, A. Yencha, A. Juarez, S. Cavanagh, P. Bolognesi, and G. King, Chem. Phys. Lett. **474**, 41 (2009).

- [47] B. Gervais, E. Giglio, L. Adoui, A. Cassimi, D. Duflot, and M. E. Galassi, J. Chem. Phys. 131, 024302 (2009).
- [48] Z. L. Streeter, F. L. Yip, R. R. Lucchese, B. Gervais, T. N. Rescigno, and C. W. McCurdy, Phys. Rev. A 98, 053429 (2018).
- [49] S. Koh, K. Yamazaki, M. Kanno, H. Kono, and K. Yamanouchi, Chem. Phys. Lett. 742, 137165 (2020).
- [50] K. Henrichs, M. Waitz, F. Trinter, H. Kim, A. Menssen, H. Gassert, H. Sann, T. Jahnke, J. Wu, M. Pitzer *et al.*, Phys. Rev. Lett. 111, 113003 (2013).
- [51] E. R. Peterson and P. H. Bucksbaum, Phys. Rev. A 64, 053405 (2001).
- [52] J. Zhang, Y. Yang, Z. Li, H. Sun, S. Zhang, and Z. Sun, Phys. Rev. A 98, 043402 (2018).
- [53] M. Lein, E. K. U. Gross, and V. Engel, Phys. Rev. A 64, 023406 (2001).
- [54] M. Schmidt, K. Baldridge, J. Boatz, S. Elbert, M. Gordon, J. Jensen, S. Koseki, N. Matsunaga, K. Nguyen, S. Su, T. Windus, M. Dupuis, and J. Montgomery Jr., J. Comput. Chem. 14, 1347 (1993).